Electronic Supplementary Material (ESI) for Journal of Materials Chemistry A.

A unique approach in designing resilient bi-functional nano-electrocatalysts based on ultrafine bimetallic nanoparticles dispersed in carbon nanospheres

Ravi Nandan,[a] and Karuna Kar Nanda*[a]

[a] *Materials Research Centre, Indian Institute of Science, Bangalore – 560012, India. Fax: +91-80-2360 7316 ; Tel: +91-080-2293 2996;*
**E-mail: nanda@mrc.iisc.ernet.in*

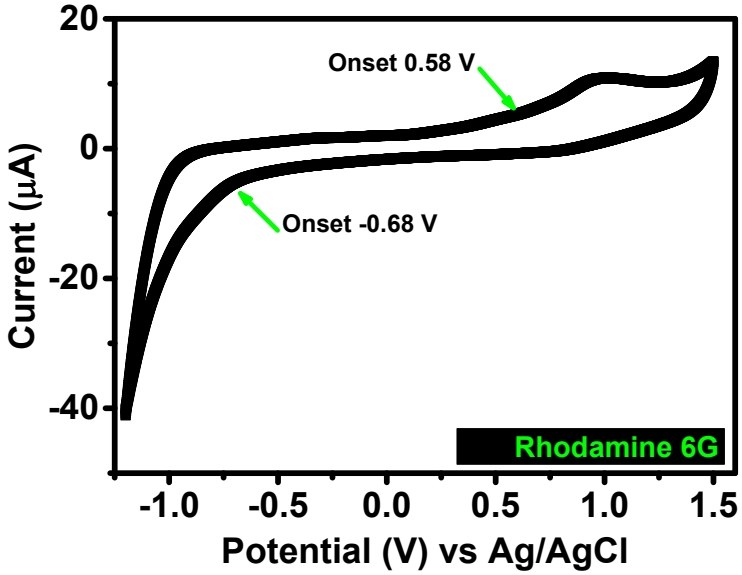

Figure S1. Cyclic voltammogram of rhodamine 6G in acetonitrile containing tetrabutylammonium perchlorate as the supporting electrolyte.

To estimate the HOMO and LUMO energy levels of rhodamine 6G (R6G), Cyclic voltammogram was recorded using a traditional three-electrode system, consisting of glassy carbon electrode coated with R6G as the working electrode, KCl saturated Ag/AgCl as the reference electrode and platinum wire as the counter electrode. Experiment was carried in acetonitrile containing 0.4 mM tetrabutylammonium perchlorate (from Sigma Aldrich) as the supporting electrolyte. The energy levels (HOMO and LUMO) in eV of R6G were evaluated according to the following equations as reported in literature[1]

$$E_{HOMO} = -e(E_{oxd(onset)} + 4.4) \quad (1)$$

$$E_{LUMO} = -e(E_{red(onset)} + 4.4) \quad (2)$$

where E_{oxd} (~0.58 V) and E_{red} (~ -0.68 V) represent the onset of oxidation and reduction potential, respectively, obtained from recorded CV. The corresponding calculated HOMO and LUMO levels are -4.98 and -3.72 eV, respectively.

Thus the HOMO of R6G is 0.46 V above the potential of standard hydrogen electrode (SHE) and it is well above the reduction potentials of $[PdCl_4]^{2-}$ (0.591 V vs SHE) and $[PtCl_4]^{2-}$ (0.775 V vs SHE), respectively.[2] The relative potential levels as discussed vindicate the possible spontaneous reduction of metal ions when mixed with R6G solution.

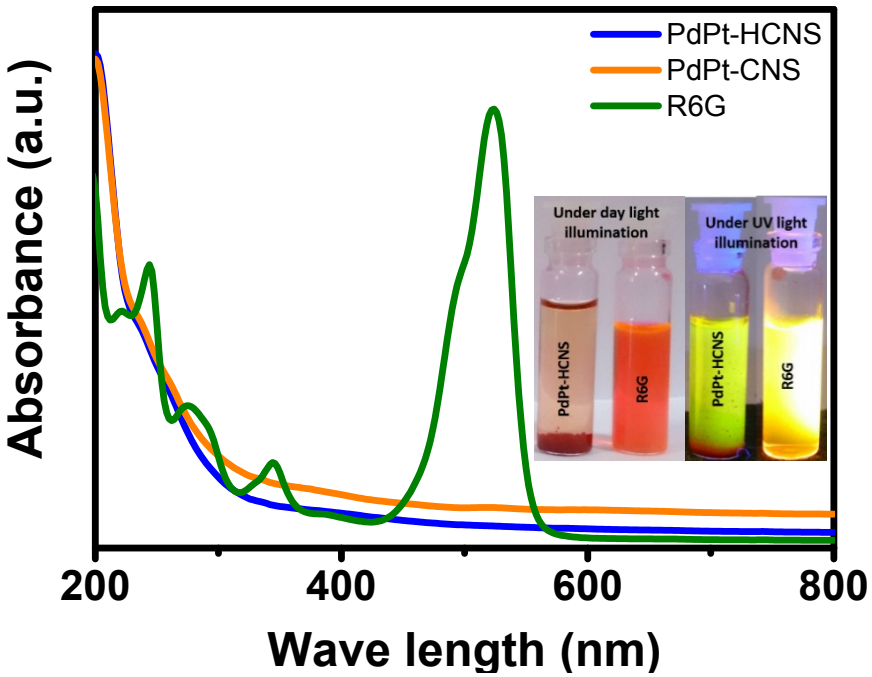

Figure S2. Absorbance spectrum of rhodamine 6G (R6g), PdPt-CNS and PdPt-HCNS in aqueous media. Inset show optical photographs of PdPt-HCNS and R6G under day and UV light illumination.

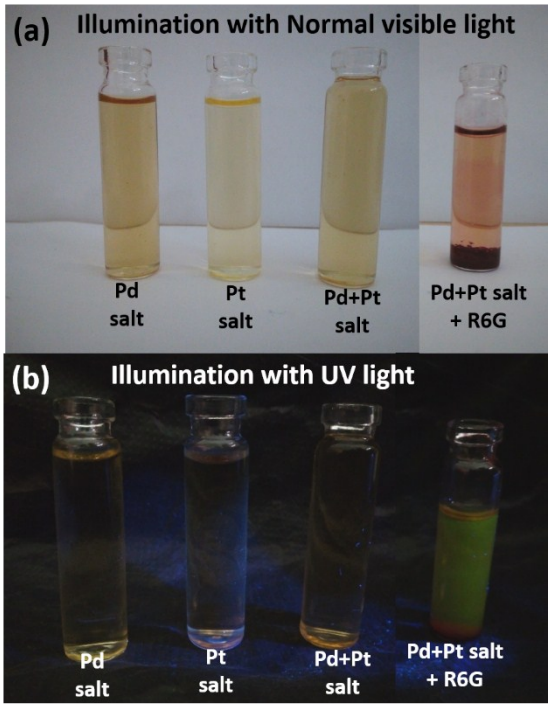

Figure S3. Optical photographs of Pd, Pt, Pd+Pt aqueous salt solutions and PdPt-HCNS (R6G+Pd+Pt) under illumination of (a) normal visible day and (b) UV light.

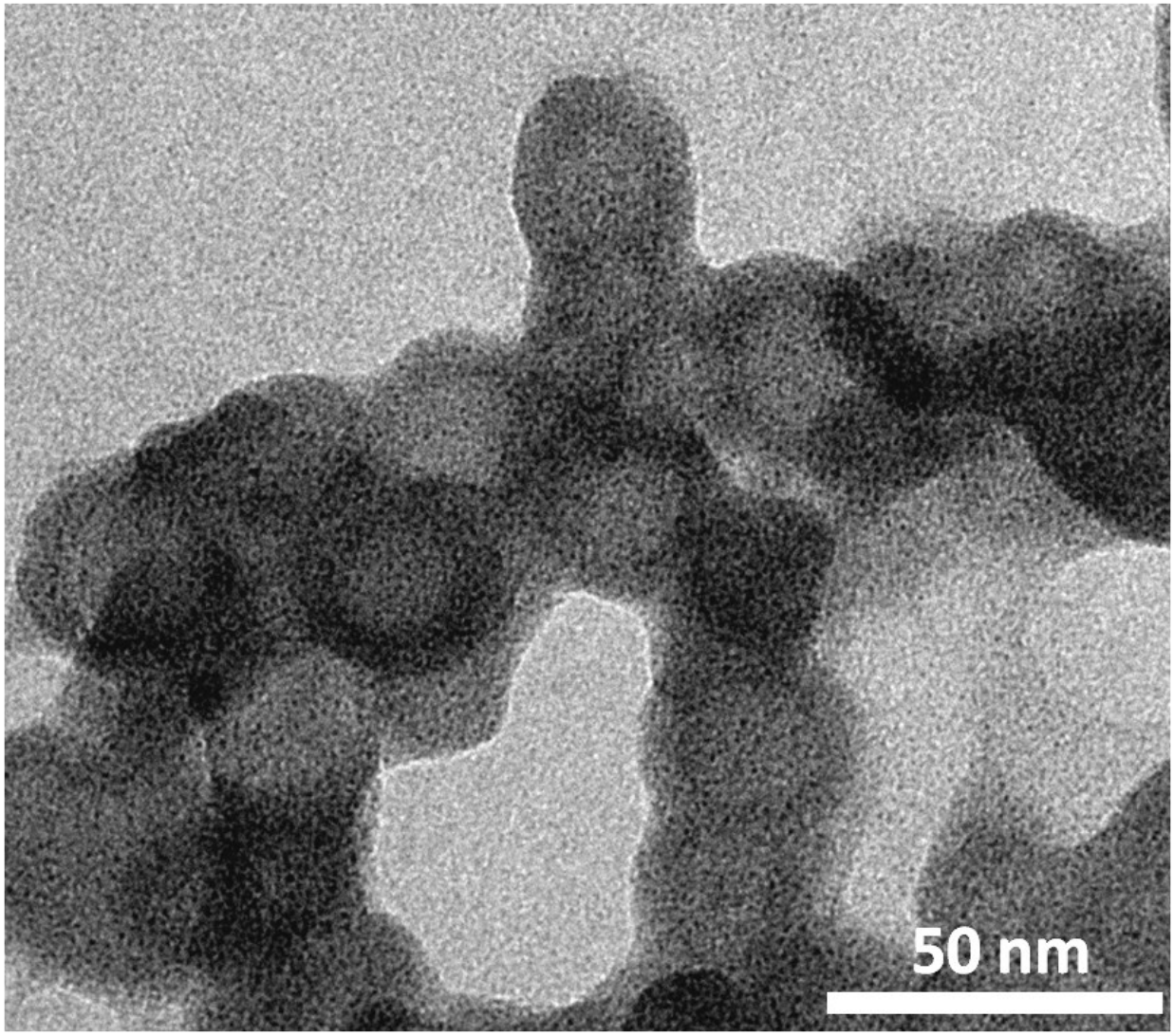

Figure S4. TEM image of PdPt-HCNS.

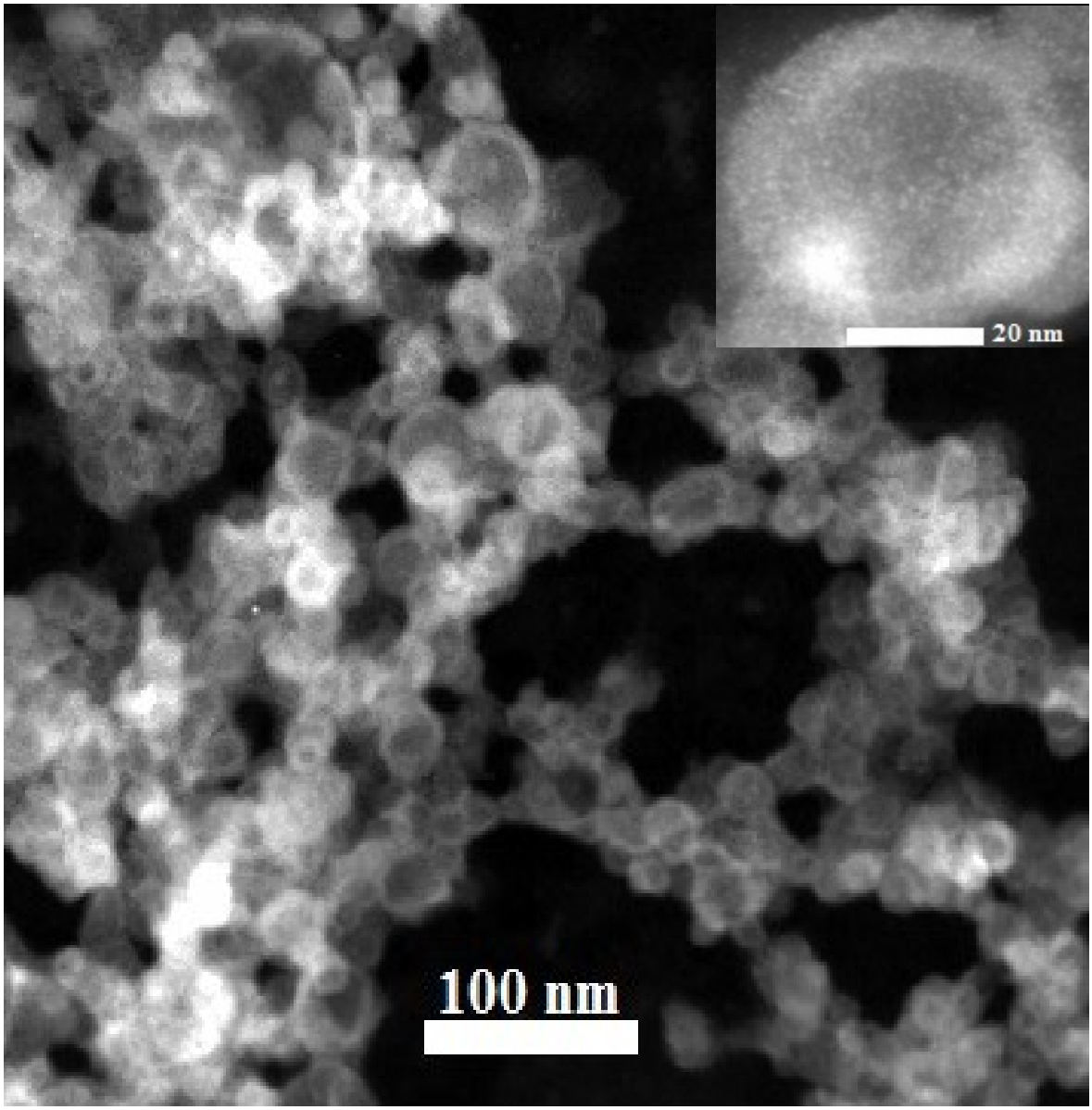

Figure S5. STEM-HAADF image of PdPt-HCNS. Inset shows the magnified image.

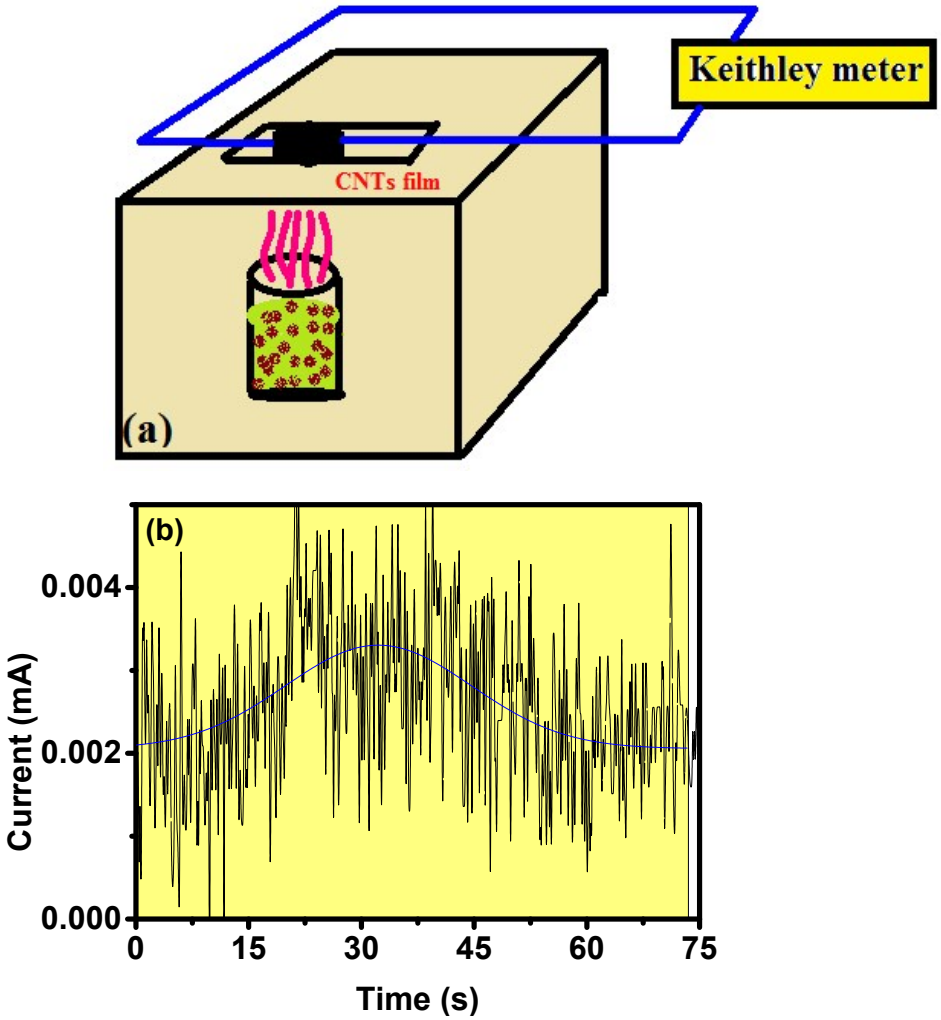

Figure S6. (a) Schematic of gas sensing set-up using CNTs film during synthesis of PdPt-HCNS, (b) current response during synthesis of PdPt-HCNS.

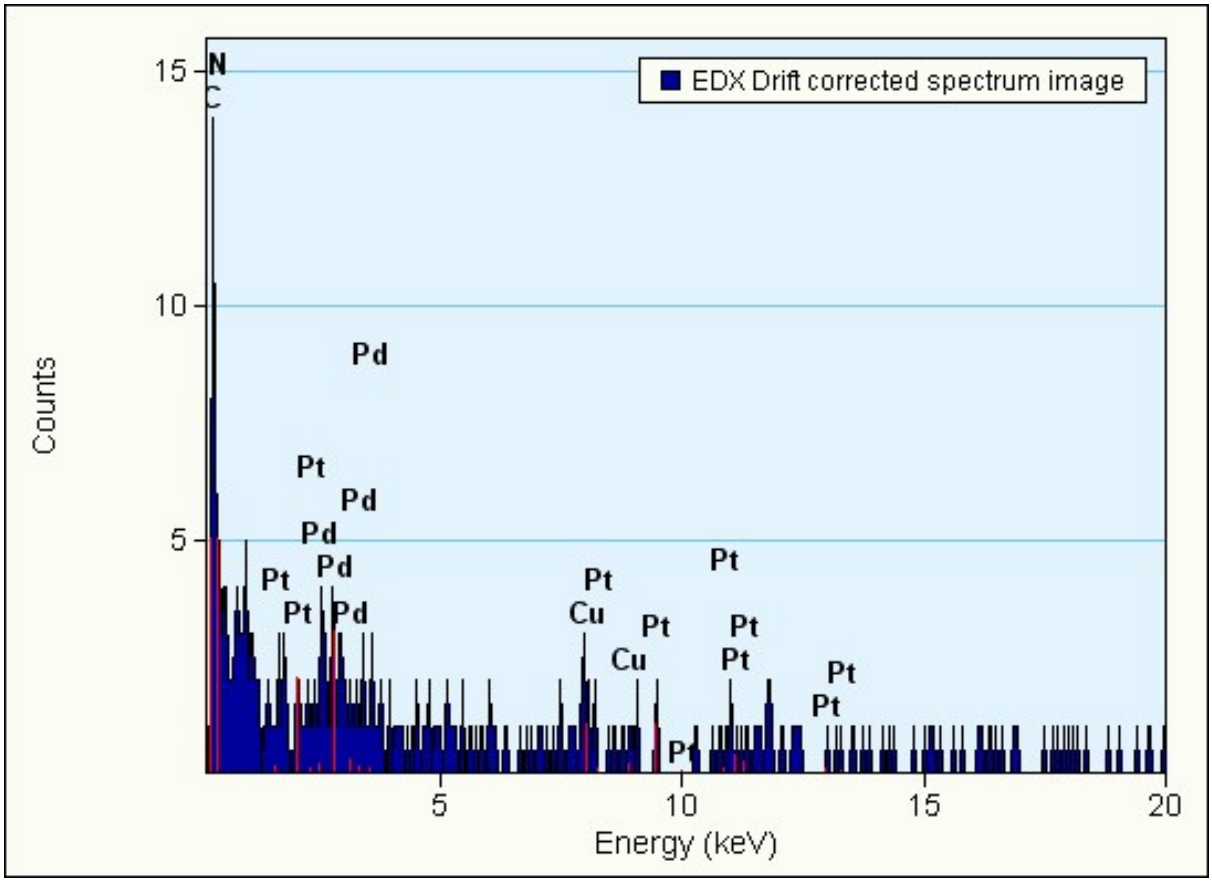

Figure S7. EDS spectrum of PdPt-HCNS

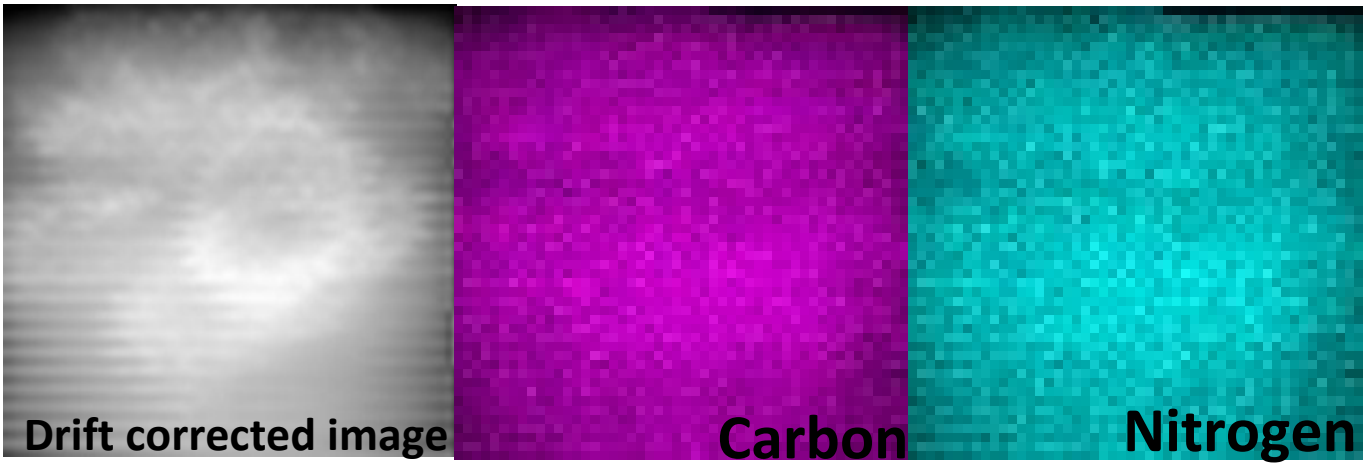

Figure S8. Drift corrected image of PdPt-HCNS and corresponding elemental mapping of carbon and nitrogen in HCNS.

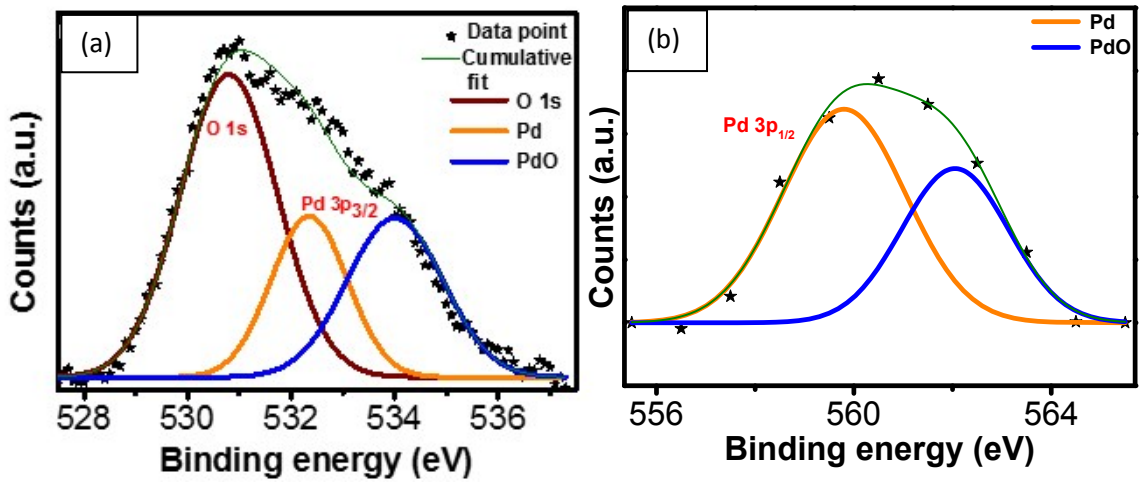

Figure S9. Deconvulated core spectrum of (a) O 1s & Pd $3p_{3/2,}$ (b) $Pd3p_{1/2}$ in PdPt-HCNS.

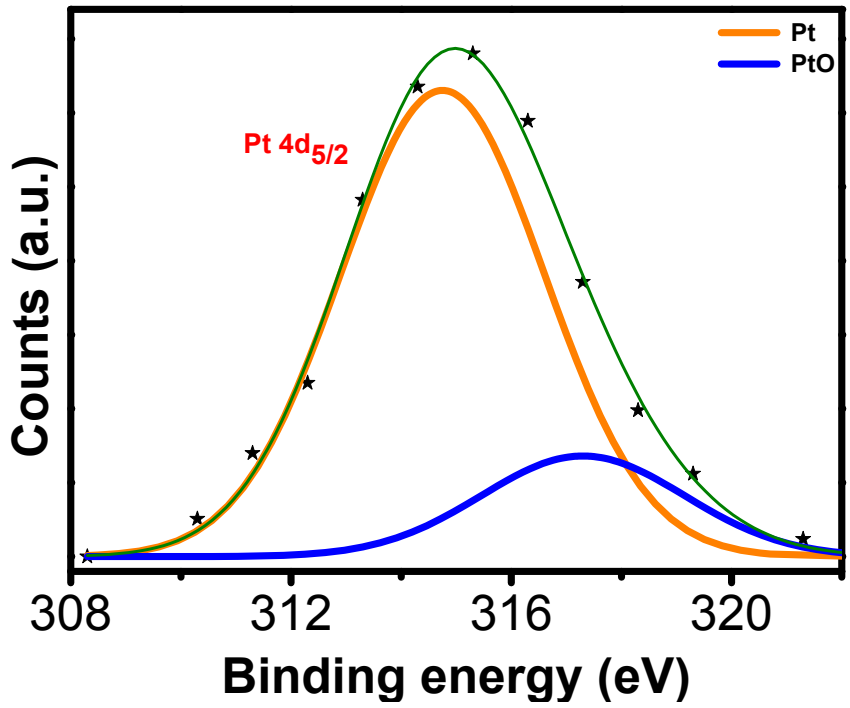

Figure S10. Deconvulated core spectrum of $Pt4d_{5/2}$ in PdPt-HCNS.

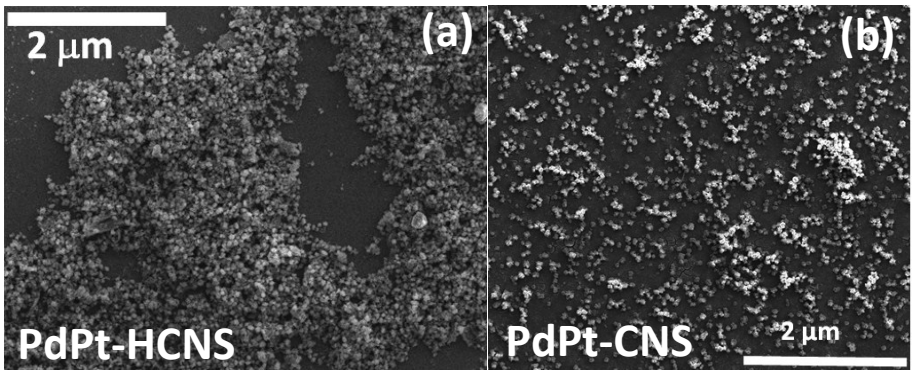

Figure S11 (a,b). Scanning electron microscopic image of PdPt-HCNS & PdPt-CNS, respectively, drop casted on silicon substrate.

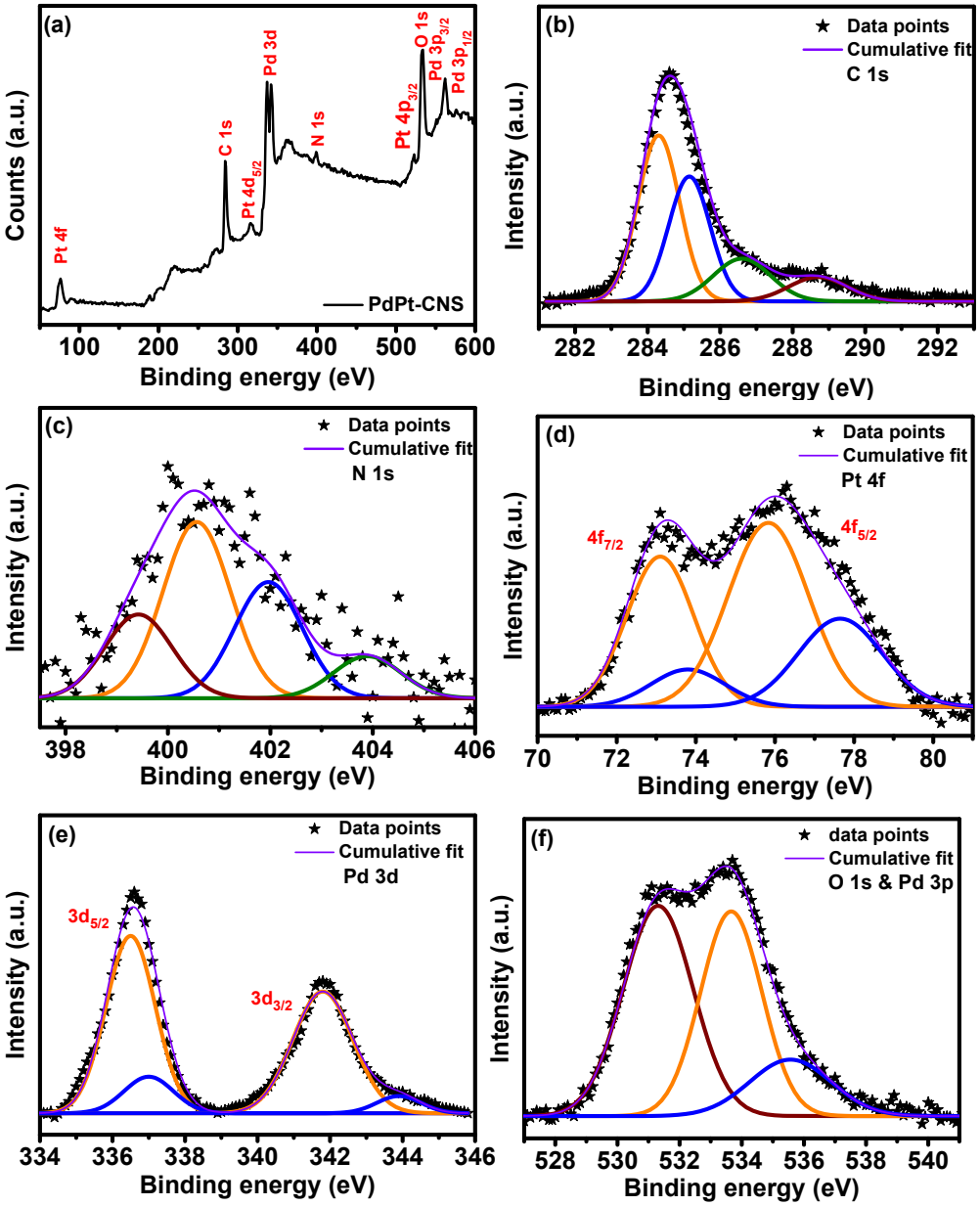
(a)
Counts (a.u.)
Binding energy (eV)
Pt 4f
C 1s
Pt 4d5/2
Pd 3d
N 1s
Pt 4p3/2
O 1s
Pd 3p3/2
Pd 3p1/2
PdPt-CNS
(b)
Intensity (a.u.)
Binding energy (eV)
Data points
Cumulative fit
C 1s
(c)
Intensity (a.u.)
Binding energy (eV)
Data points
Cumulative fit
N 1s
(d)
Intensity (a.u.)
Binding energy (eV)
Data points
Cumulative fit
Pt 4f
4f7/2
4f5/2
(e)
Intensity (a.u.)
Binding energy (eV)
Data points
Cumulative fit
Pd 3d
3d5/2
3d3/2
(f)
Intensity (a.u.)
Binding energy (eV)
data points
Cumulative fit
O 1s & Pd 3p

Figure S12. (a) Survey spectrum of PdPt-CNS and core spectra of (b) C 1s, (c) N 1s, (d) Pt 4f, (e) Pd 3d and (f) Pd 3p & O1s for PdPt-CNS

Figure (a) shows the wide spectrum of PdPt-CNS which consist of Pt (4f, 4d & 4p), C (1s), Pd (3d & 3p), N (1s) and O (1s) peaks. The deconvulated C 1s spectrum (fig. b) consists of peaks around 284.3 (-C=C-), 285.16 (C-N) with 286.6 & 288.62 eV (different modes of C-O interactions). The peak at about 400 eV (N 1s, figure 4c) is deconvoluted into four constituent peaks around 399.44 , 400.5eV correspond to nitrile-, quaternary-type while peaks around 402 and 403.9 eV represents different forms of oxides of nitrogen species in CNS. Further, peaks in figure (d) represent the profile of Pt $4f_{7/2}$ (73.11 eV), Pt $4f_{5/2}$ (75.11 eV) and Pt $4f_{7/2}$ (73.77 eV), Pt $4f_{5/2}$ (77.64 eV) are assigned to Pt^0 and Pt^{2+} species, respectively. The intense peaks of Pd 3d and 3p are deconvoluted (Fig. e) to identify the valence states. The peaks at 336.5 eV (Pd $3d_{5/2}$), 341.7 eV (Pd $3d_{3/2}$) along with 337 eV (Pd $3d_{5/2}$), 343.9 eV (Pd $3d_{3/2}$) correspond to metallic (Pd^0) and higher (Pd^{2+}) states, respectively. Moreover, the peaks at 533.6 eV (Pd $3p_{3/2}$) and 535.6 eV (Pd $3p_{3/2}$) as shown in figure (f) are assigned to Pd^0 and Pd^{2+} states. The peak at 531.3 eV (O 1s) corresponds to the oxygen which may arise due to C-O / N-O_x moieties in consort with the adsorption at Pd surface, if any. The slight shift in the binding energies of Pt-/Pd- states in the deconvoluted high resolution core spectrum can be attributed to the electronic modifications due to bimetallic nature of PdPt-CNS which similar to that of PdPt-HCNS.

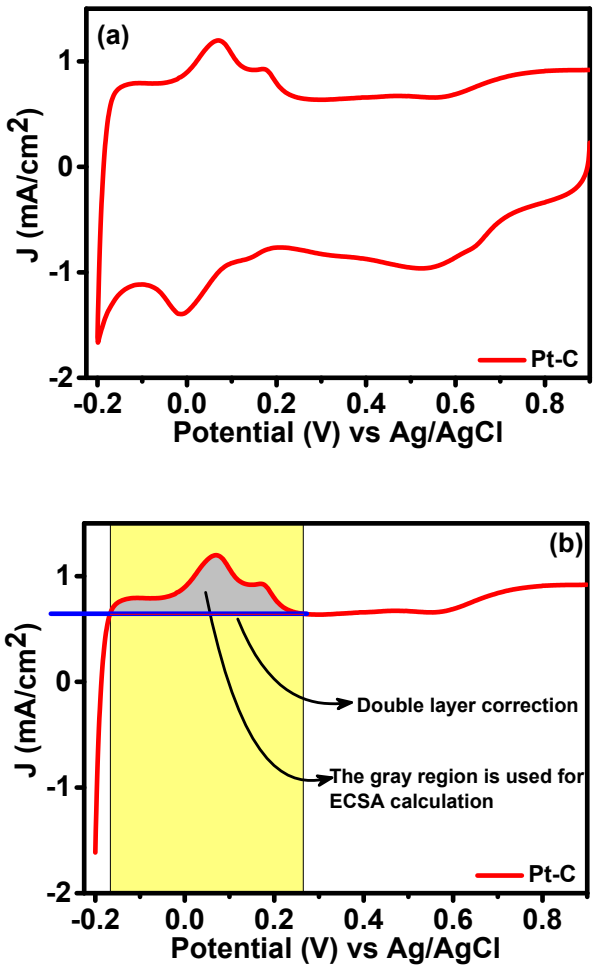

Figure S13. (a) CV of Pt-C in nitrogen degassed 0.5 M H_2SO_4aqueous solution, scanned from -0.2 to 0.9 V then back to -0.2 V, with a scan rate of 50 mV/s. (b) gray region is used to calculate the ECSA for Pt-C.

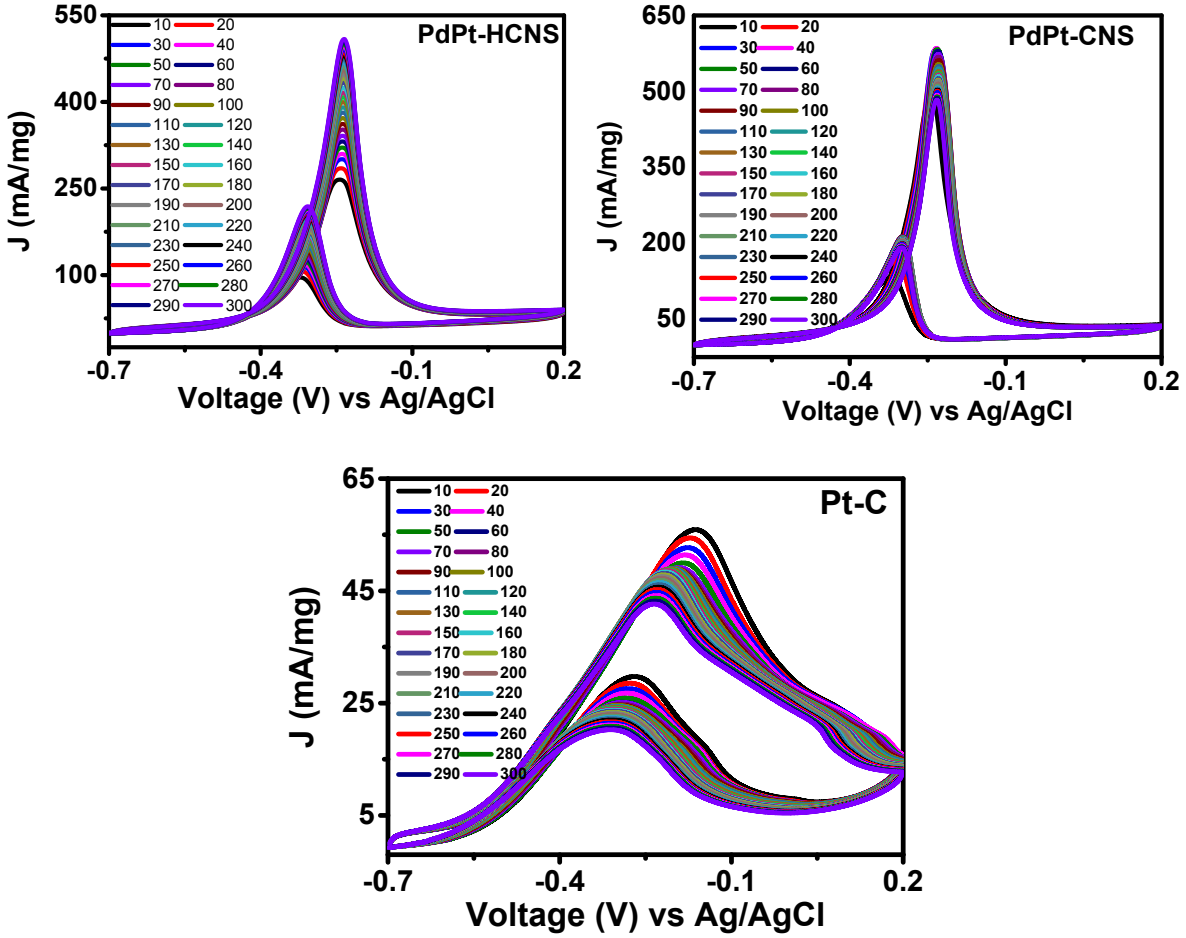

Figure S14. Cyclic voltammogram of methanol (0.5 M) electro-oxidation in alkaline media (1 M NaOH) using PdPt-HCNS, PdPt-CNS and commercial state-of-the-art Pt-C catalysts under similar experimental conditions.

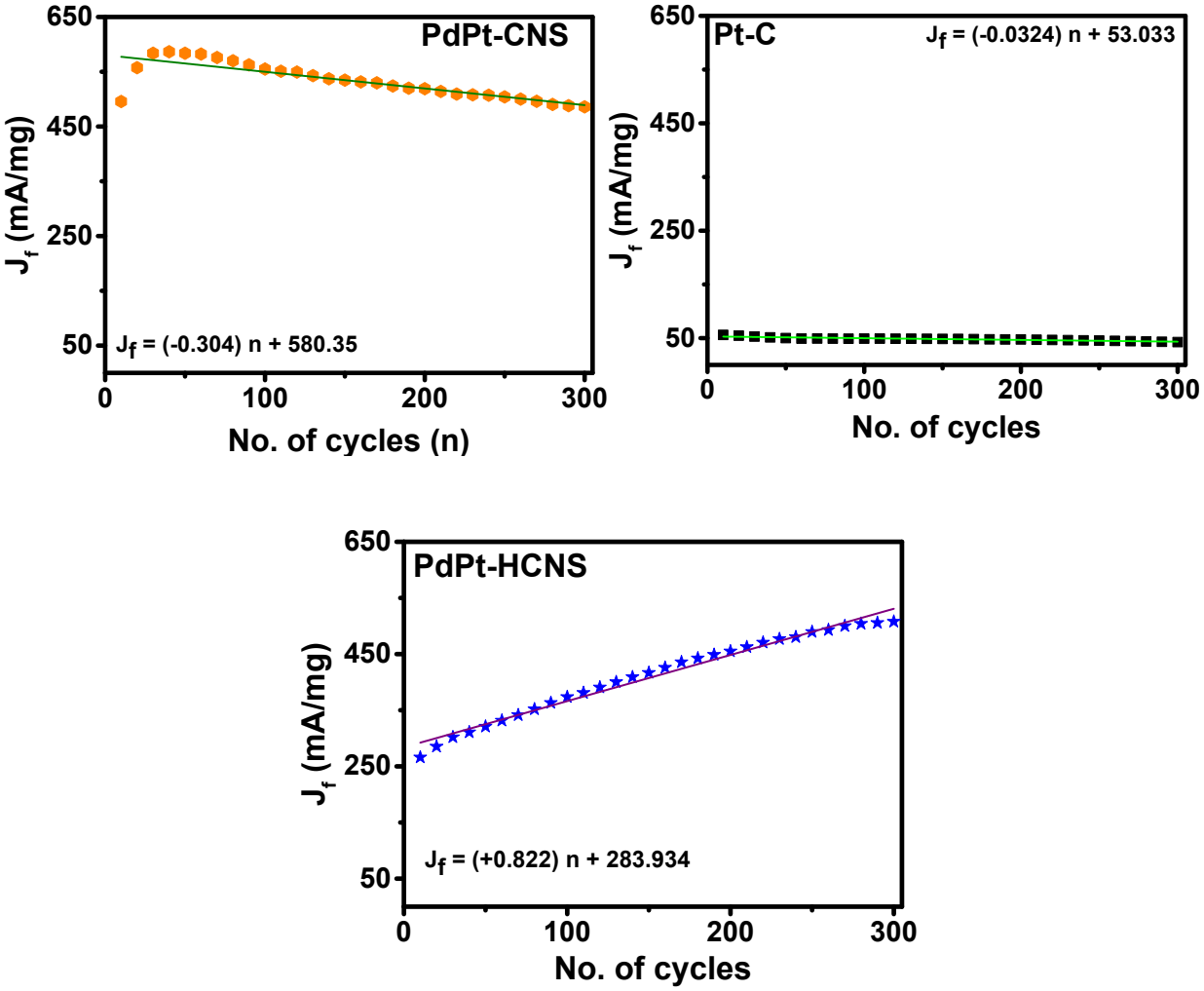

Figure S15. (dJ_f/dn) The rate of change of forward current density (J_f) with no. of cycles (n) for PdPt-CNS, Pt-C and PdPt-HCNS for MOR.

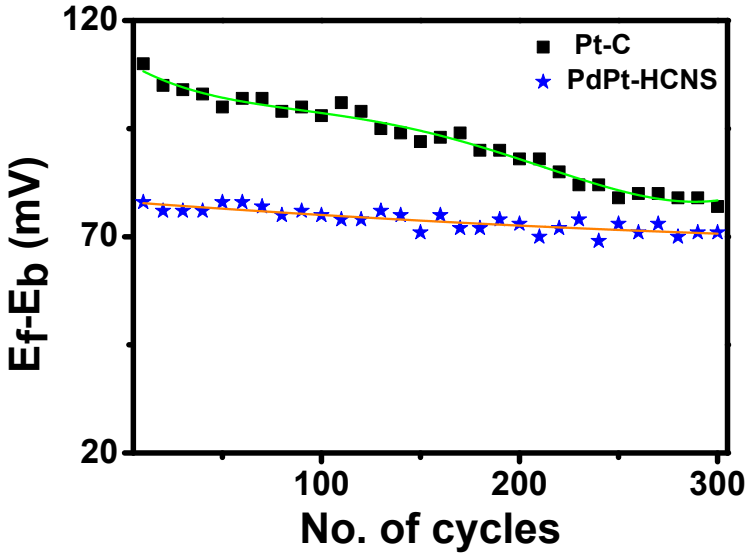

Figure S16. Forward (E_f) and reverse (E_b) peak potential separation (E_f- E_b) with no. of cycles for PdPt-HCNS and commercial state-of-the-art Pt-C catalyst for MOR.

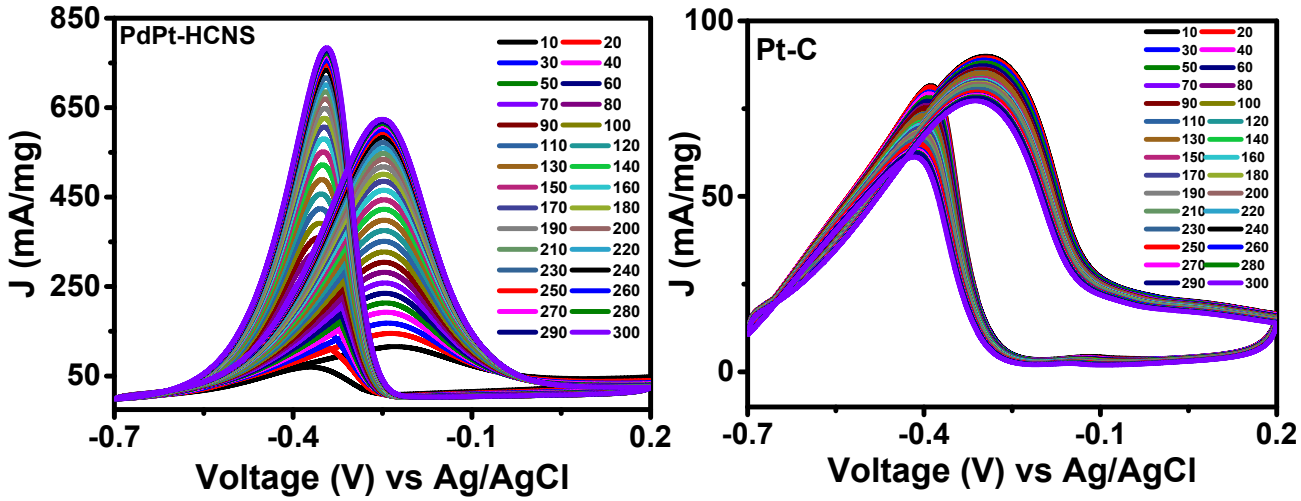

Figure S17. Cyclic voltammogram of ethanol (0.5 M) electro-oxidation in alkaline media (1 M NaOH) using PdPt-HCNS and commercial state-of-the-art Pt-C catalysts under similar experimental conditions.

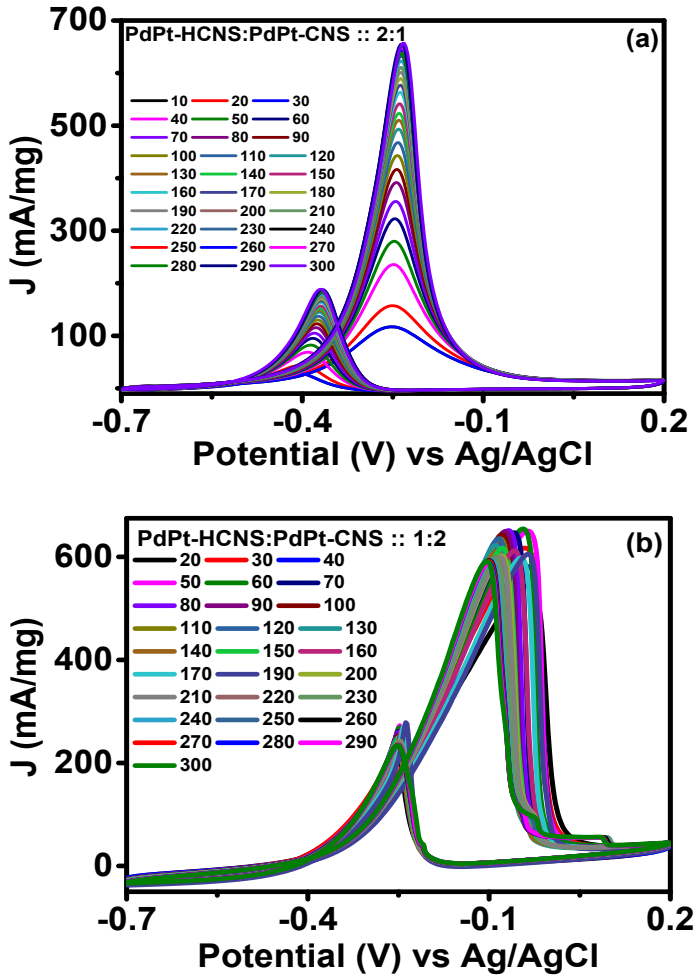

Figure S18. Cyclic voltammogram of methanol (0.5 M) electro-oxidation in alkaline media (1 M NaOH) using (a,b) PdPt-HCNS:PdPt-CNS :: 2:1 and 1:2, respestively.

Table S1. Mass activity for methanol electro-oxidation in alkaline media using various mono-/multi- metallic catalyst.

Catalyst composition	Testing conditions	Mass activity	Ref.
Pt/Y-zeolite (Y)/Vulcan XC-72R	0.1 M KOH and 1 M CH_3OH, 100 mVs^{-1}	7 mA mg^{-1}	3
Pt/ceria nano rods	0.5 M KOH and 1 M CH_3OH, 100 mVs^{-1}	25 mA mg^{-1}	4
Pt–Sn	1 M KOH and 1 M CH_3OH, 10 mVs^{-1}	100 mA mg^{-1}	5
Pd/Fe_3O_4/GC	0.1 M NaOH and 1 M CH_3OH 50 mVs^{-1}	110 mA mg^{-1}	6
Pd/SnO_2–TiO_2/MWCNT	0.5 M NaOH and 1 M CH_3OH, 20 mVs^{-1}	114 mA mg^{-1}	7
Pt-on-Pd-on-Au/CNTs	1 M NaOH and 1 M CH_3OH, 50 mVs^{-1}	147 mA mg^{-1}	8
Pt/G–V(C, N)	1 M KOH and 2 M CH_3OH, 50 mVs^{-1}	210 mA mg^{-1}	9
CuxPdy/C	0.5 M KOH and 0.5 M CH_3OH, 50 mVs^{-1}	220 mA mg^{-1}	10
np-Pd	1 M KOH and 0.5 M CH_3OH, 10 mVs^{-1}	223.52 mA mg^{-1}	11
Pd–NiO/C	1 M KOH and 1 M CH_3OH, 10 mVs^{-1}	250 mA mg^{-1}	12
Pd/graphene	0.5 M NaOH and 1 M CH_3OH, 50 mVs^{-1}	283 mA mg^{-1}	13
Pd/PPY/graphene	0.5 M NaOH and 1 M CH_3OH, 50 mVs^{-1}	359.8 mA mg^{-1}	14
PdMo/CNT	1 M KOH and 1 M CH_3OH, 50 mV s^{-1}	395.6 mA mg^{-1}	15
PdCuSn/CNTs	1 M KOH and 0.5 M CH_3OH, 50 mVs^{-1}	395.94 mA mg^{-1}	16
Pt/WO_3/MC	0.5 M NaOH and 1 M CH_3OH, 25 mVs^{-1}	410 mA mg^{-1}	17
Pd/MnO_2/CNT	0.5 M NaOH and 1 M CH_3OH, 50 mVs^{-1}	432.02 mA mg^{-1}	18
PtNi/POMA/GE/GC	1 M KOH and 1 M CH_3OH, 50 mVs^{-1}	520.5 mA mg^{-1}	19
PtNi/C	1 M NaOH and 1 M CH_3OH, 50 mV s^{-1}	559 mA mg^{-1}	20
PdNi/C	1 M KOH and 1 M CH_3OH, 50 mVs^{-1}	575 mA mg^{-1}	21
Pt-PdCo/P-MWCNTs	0.1 M KOH and 1 M CH_3OH, 20 mVs^{-1}	575 mA mg^{-1}	22
$Ti_{30}Cu_{60}Pd_{10}$	0.5 M NaOH and 1 M CH_3OH, 25 mVs^{-1}	577.85 mA mg^{-1}	23
PtAu/PDA-RGO	1 M KOH and 1 M CH_3OH, 50 mVs^{-1}	645.1 mA mg^{-1}	24
Pd/TiO_2–C	0.5 M KOH and 1 M CH_3OH, 5 mVs^{-1}	650 mA mg^{-1}	25
PdPt-HCNS +PdPt-CNS	**1 M NaOH and 1 M CH_3OH, 50 mVs^{-1}**	**660 mA mg^{-1}**	**Present Study**

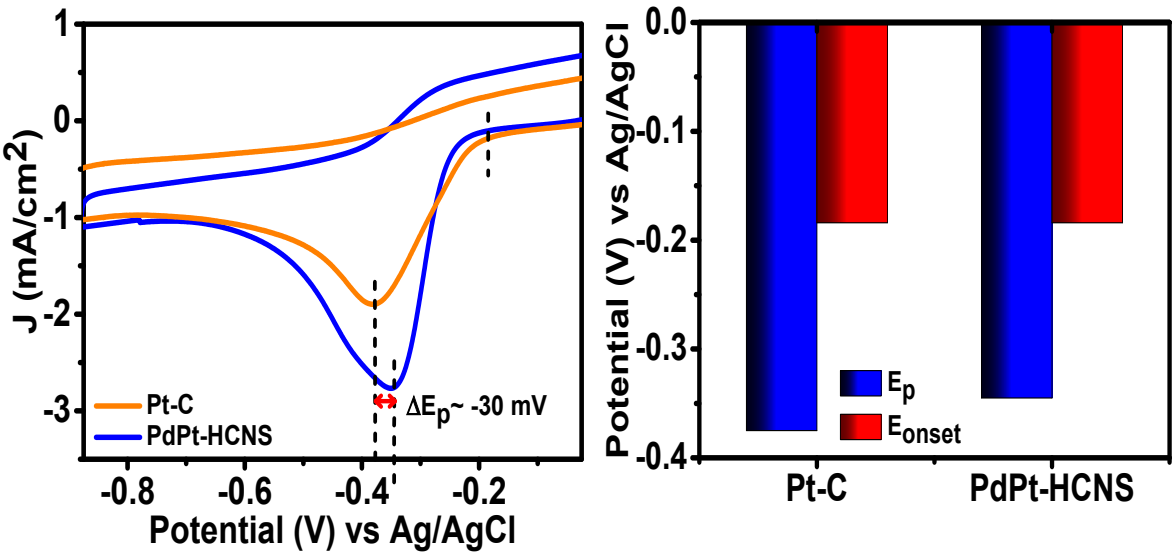

Figure S19. (a) CV of PdPt-HCNS and Pt-C (20 wt. %) at 50 mVs^{-1} for ORR. (b) Shows the onset potential (E_{onset}) and peak potential (E_p) for Pt-C and PdPt-HCNS, respectively, for ORR.

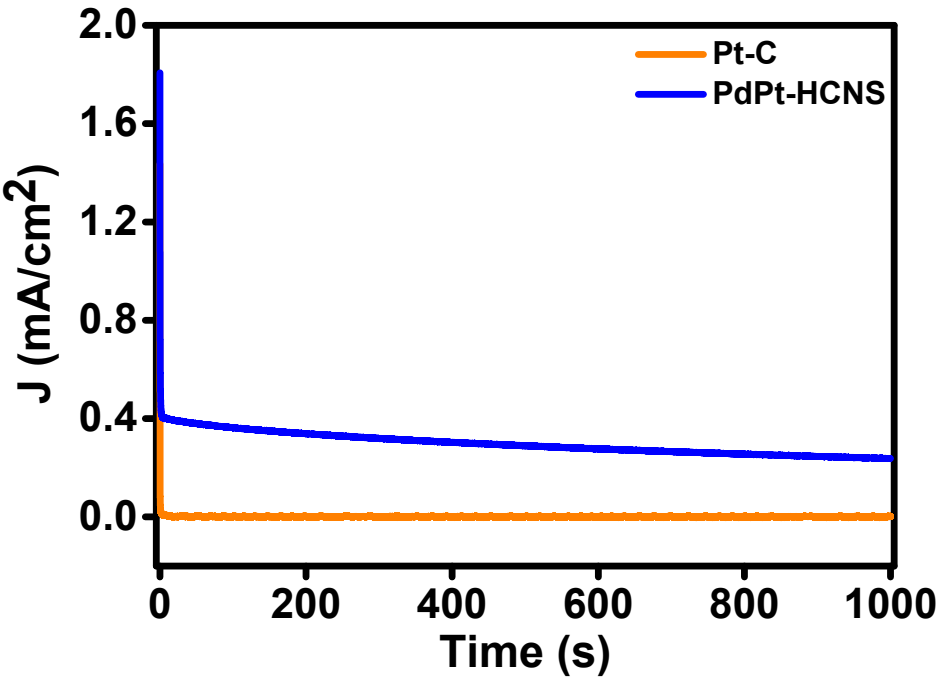

Figure S20. Chronoamperometry study at -0.340 V in alkaline media (1 M NaOH) using PdPt-HCNS and commercial state-of-the-art Pt-C catalysts.

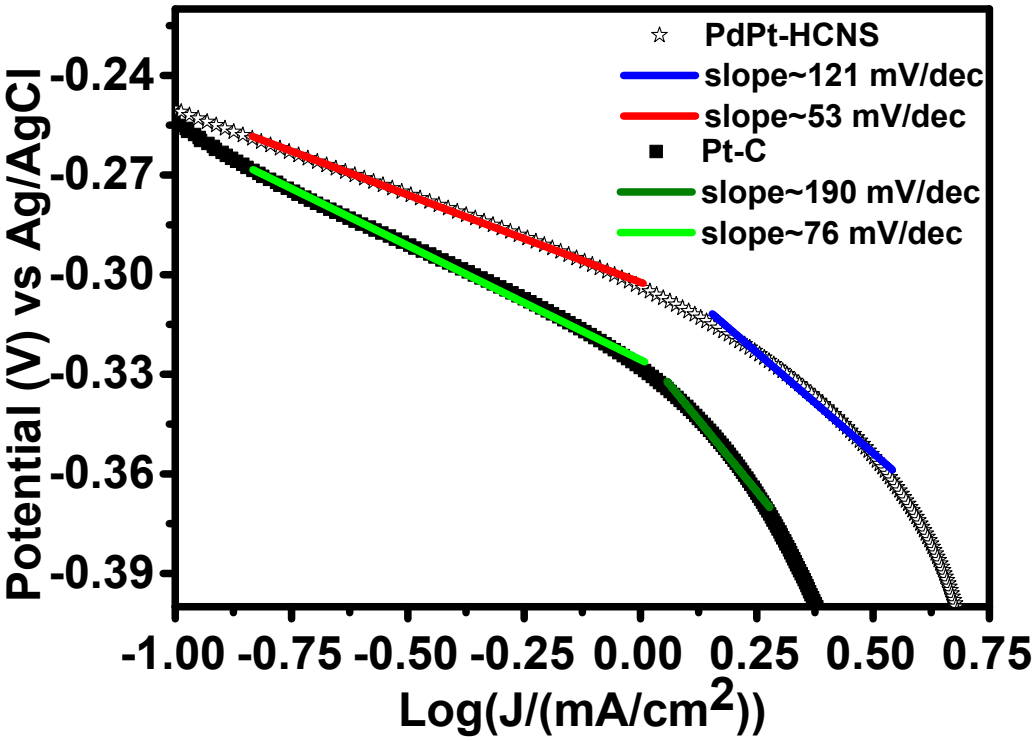

Figure S21. Tafel slope derived from the RDE polarization curve (figure 8a) for PdPt-HCNS and Pt-C catalysts.

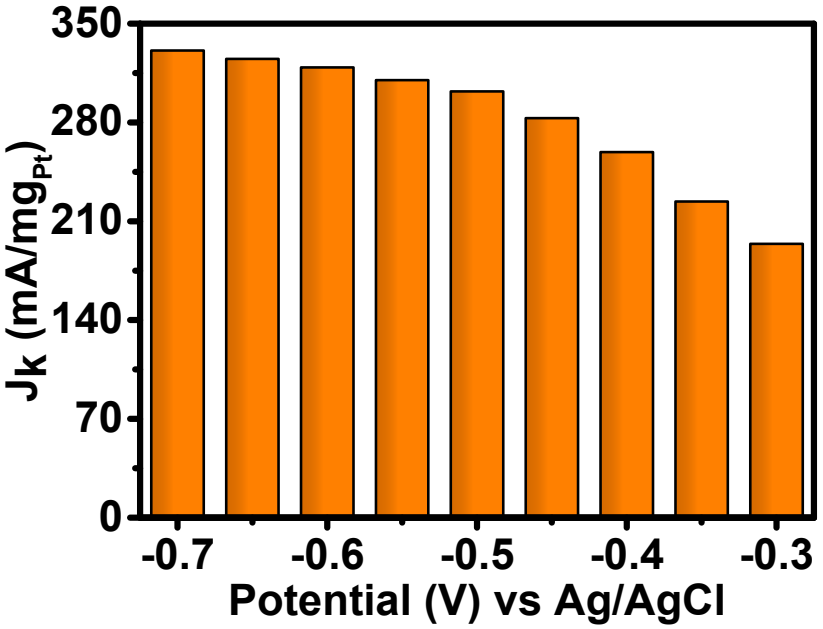

Figure S22. Normalized kinetic current density (J_k) with respect to Pt loading at different potential obtained from the intercept of corresponding K-L plots in mixed control region for PdPt-HCNS catalyst.

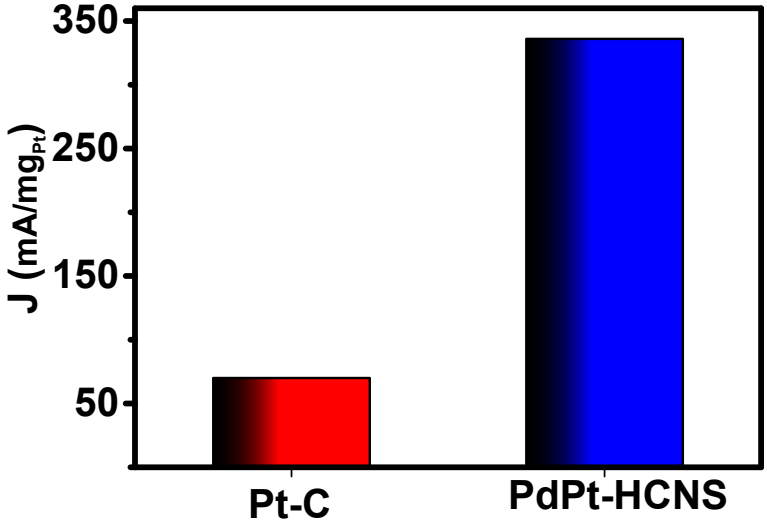

Figure S23. Normalized measured current density with respect to Pt loading at -0.7 V (vs Ag/AgCl reference electrode) for ω = 2000 rpm for commercial state-of-the-art Pt-C and PdPt-HCNS catalysts, respectively.

Table S2. Mass activity and Tafel slope in low over-potential region for ORR in alkaline media using various mono-/multi- metallic catalyst.

Catalyst	**Tafel Slope** (Near lower over-potentials)	**Experimental conditions** (electrolyte, rpm, scan speed & potential)	**Measured ORR Current density** (mA/mg_{Pt})	**References**
Pt/(Pt+C)	81	1 M NaOH, 1600 rpm, 10 mV/s, -0.06 V vs Hg/HgO	89.6	*Electrochimica Acta,* 1998, **44,** 1317-1327.
$Pt_{0.6}$^Ag-B/C		0.5 M KOH, 1600 rpm, 10 mV/s, -0.7 V vs NHE	325	*Phys. Chem. Chem. Phys.*, 2011, **13**, 3863–3872.
Hydrogenated-Pt/$CaMnO_3$	65	0.1 M KOH, 1600 rpm, 5 mV/s, 0.85 V vs RHE	380	*Adv. Mater.* 2014, **26**, 2047–2051
Pt-coated Pd nanocube		1 M NaOH, 1600 rpm, 10 mV/s, 0.6 V vs RHE	50	*Journal of Power Sources,* 2014, **268**, 712-717.
$Pt_{76}Co_{24}$	60	1 M NaOH, 1600 rpm, 10 mV/s, -0.6 V vs SCE	70	*Phys. Chem. Chem. Phys*., 2014, **16**, 19298-19306.
CuPt-Nanocage	69.94	0.1 M KOH, 1600 rpm, 10 mV/s, 0.5 V vs RHE	122	*ACS Catal.,* 2015, **5**, 1445−1452
Pt-C (Commercial, 20 % Pt loading)	76	1 M NaOH, 1600 rpm, 10 mV/s, -0.8 V vs Ag/AgCl	71	This work
PdPt-HCNS	53	1 M NaOH, 1600 rpm, 10 mV/s, -0.8 V vs Ag/AgCl	336	Thiswork

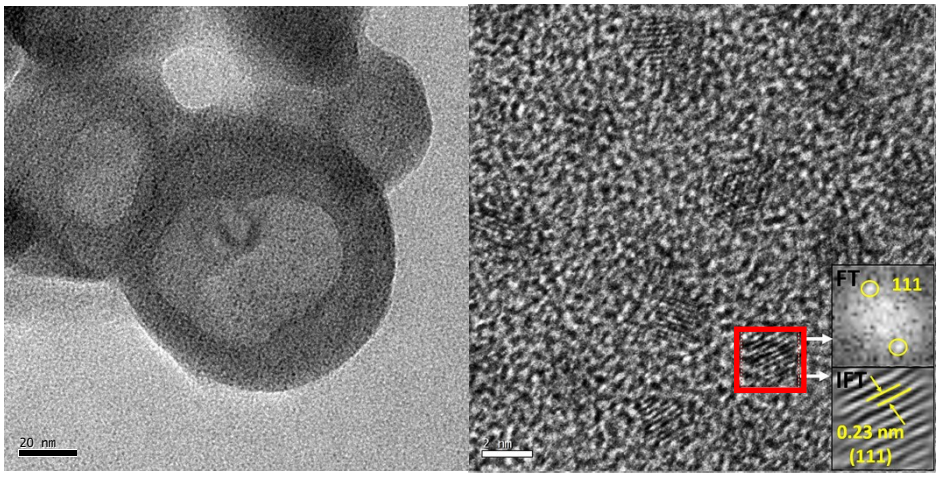

Figure S24. (a) TEM and (b) HRTEM images of PdPt-HCNS, inset of figure b show FT and inverse FT patterns (deduced from FT pattern) for a PdPt bimettalic nanoparticle after ORR accelerated stability test.

References

1. V. Gupta, N. Chaudhary, R. Srivastava, G. Datt Sharma, R. Bhardwaj and S. Chand, *J. Am. Chem. Soc*, 2011, **133**, 9960.
2. H. C. Choi, M. Shim, S. Bangsaruntip and H. Dai, *J. Am. Chem. Soc* ,2002, **124**, 9058.
3. A. Suleiman, C. L. Menendez, R. Polanco, E. R. Fachini, Y. Hernandez-Lebron, M. J. F. Guinel, R. Roque-Malherbe and C. R. Cabrera, *RSC Adv,* 2015, **5**, 7637.
4. Y. Zhou, C. L. Menendez, M. J. F. Guinel, E. C. Needels, I. Gonzalez-Gonzalez, D. L. Jackson, N. J. Lawrence, C. R. Cabrera and C. L. Cheung, *RSC Adv,* 2014, **4**, 1270.
5. E. E. Switzer, T. S. Olson, A. K. Datye, P. Atanassov, M. R. Hibbs and C. Cornelius, J. *Electrochim Acta,* 2009, **54**, 989.
6. J. Li, J. Ren, G. Yang, P. Wang, H. Li, X. Sun, L. Chen, J.-T. Ma and R. Li, *Mater. Sci. Eng.,* 2010, **172**, 207.
7. H. An, L. Pan, H. Cui, B. Li, D. Zhou, J. Zhai and Q. Li, *Electrochim Acta,* 2013, **102**, 79.
8. R. Shi, J. Wang, N. Cheng, X. Sun, L. Zhang, J. Zhang and L. Wang, *Electrochim Acta,* 2014, **148**, 1.
9. T. Huang, S. Mao, G. Zhou, Z. Zhang, Z. Wen, X. Huang, S. Ci and J. Chen, *Nanoscale,* 2015, **7**, 1301.
10. H. Mao, T. Huang and A. Yu, *Electrochim Acta,* 2015, **174**, 1.
11. X. Wang, W. Wang, Z. Qi, C. Zhao, H. Ji and Z. Zhang, *J. Power Sources,* 2010, **195**, 6740.
12. K.-H. Ye, S.-A. Zhou, X.-C. Zhu, C.-W. Xu and P. K. Shen, *Electrochim Acta,* 2013, **90**, 108.
13. H. Huang and X. Wang, *J. Mater. Chem,* 2012, **22**, 22533.
14. Y. Zhao, L. Zhan, J. Tian, S. Nie and Z. Ning, *Electrochim Acta,* 2011, **56**, 1967.
15. N. Kakati, J. Maiti, S. H. Lee and Y. S. Yoon, *Int.l J. Hydrogen. Energy,* 2012, **37**, 19055.
16. F. Zhu, G. Ma, Z. Bai, R. Hang, B. Tang, Z. Zhang and X. Wang, *J. Power Sources,* 2013, **242**, 610.
17. J. Zeng, C. Francia, C. Gerbaldi, V. Baglio, S. Specchia, A. S. Aricò, P. Spinelli, *Electrochim Acta,* 2013, **94**, 80.
18. Y. Zhao, L. Zhan, J. Tian, S. Nie and Z. Ning, *Int.l J. Hydrogen. Energy,* 2010, **35**, 10522.
19. F. Ren, H. Wang, M. Zhu, W. Lu, P. Yang and Y. Du, *RSC Adv* 2014, **4**, 24156.
20. Q. Jiang, L. Jiang, H. Hou, J. Qi, S. Wang and G. Sun, *J. Phys. Chem C,* 2010, **114**, 19714.
21. Z. Liu, X. Zhang and L. Hong, *Electrochem. Commun,* 2009, **11**, 925.
22. Y. Guo, C. Hu, L. Yang, Z. Bai, K. Wang and S. Chao, *Electrochem. Commun,* 2011, **13**, 886.
23. W. Xu, S. Zhu, Z. Li, Z. Cui and X. Yang, *J. Electrochem. Soc,* 2014, **161**, F1474.
24. F. Ren, C. Zhai, M. Zhu, C. Wang, H. Wang, D. Bin, J. Guo, P. Yang and Y. Du, *Electrochim Acta,* 2015, **153**, 175.
25. L. A. Estudillo-Wong, A. M. Vargas-Gómez, E. M. Arce-Estrada and A. Manzo-Robledo, *Electrochim Acta,* 2013, **112**, 164.